Sigma J Eng Nat Sci, Vol. 41, No. 5, pp. 980–991, October, 2023

Sigma Journal of Engineering and Natural Sciences
Web page info: https://sigma.yildiz.edu.tr
DOI: 10.14744/sigma.2023.00116

Research Article

Design optimization of railgun's electromagnetic force using surrogate modelling

Habil Akansel AKYOL[1,*], Ahmet KIZILAY[1]

[1]*Department of Electronic and Communication Engineering, Yildiz Technical University, Istanbul, 34349, Türkiye*

ARTICLE INFO

Article history
Received: 27 August 2021
Revised: 09 Npvember 2021
Accepted: 25 December 2021

Keywords:
Surrogate modelling; Optimization; Railgun; Artificial Neural Networks

ABSTRACT

The railgun is an electromagnetic device that converts electrical energy to mechanical energy for accelerating the projectiles to hyper velocities, which is the main reason that railguns are becoming an increasingly popular topic of interest among the military, defense industry and scientific communities. Output force is used for evaluating the performance and the effectiveness of a railgun which is highly depended on the Railgun geometric design parameters. When a new railgun is designed, drawing the geometry, simulation and analysis stages take a long time; this study has aimed to provide an Artificial Intelligence based surrogate model for a railgun design to prevent time consuming at these stages and to make design optimization process computationally efficient. For this reason, in this paper three different rail geometries have been combined and simulated with three different armature types by using Ansys Maxwell which is based on 3-D Finite Element Method. Within the scope of this study; first of all, one of the best rail and armature pair was selected according to the efficiency. Secondly, a dataset with inputs and outputs was created by changing the geometric variables of the selected pair. Thirdly, using this dataset; six different surrogate models were trained, tuned and tested. Railgun's output force was predicted with minimum symmetric mean absolute percentage error (SMAPE) of 1.89% at the end of tests. Finally, Particle Swarm Optimization (PSO) was carried out with the surrogate model that gave the best result for modelling of a railgun design with 8.0 kNewton required output force. These optimization results were compared with the Ansys simulation outputs and found to be hand to hand. Thus, herein, a computationally efficient method for design optimization of railgun designs has been achieved using surrogate based modelling techniques.

Cite this article as: Akyol HA, Kızılay A. Design optimization of railgun's electromagnetic force using surrogate modelling. Sigma J Eng Nat Sci 2023;41(5):980–991.

INTRODUCTION

The railgun consists of two parallel conductors called rails which connected each other by a non-ferromagnetic material called armature that is also carriers of the projectiles. While the current flows through the parallel rails, it creates a magnetic field according to the well-known right-hand rule in such a way that magnetic field lines are perpendicular to the rails and the armature. This

***Corresponding author.**
*E-mail address: akyol.akansel@gmail.com

This paper was recommended for publication in revised form by Regional Editor Osman Nuri Uçan

magnetic field lines and current passing through armature produces a force, called Lorentz force which accelerates the armature along the rails [1]. A simple diagram of a railgun and Lorentz force are shown in Figure 1 below.

In order to design the most effective railgun, we need to analyze railgun key parameters such as magnetic flux density between the rails, maximum current density over the rail cross section, repulsive force acting on the rails, and inductance gradient of the rail. These parameters affect output force of the railgun, that's why it needs to be understood that how these key parameters react under different boundary conditions and variation in dimensions [2].

The analysis of these parameters during the firing is difficult and costly. Therefore, regarding simulations should be done before the production.

In recent years, many studies had been carried out for creating surrogate models using AI algorithms with high computationally efficiency to be used in design optimization or design with high performance and accuracy requirements [4,5]. Some worth mentioning published works in literature on field of surrogate based modelling of high frequency electromagnetic devices can be named as: modelling of microwave transistors [6-10], reflection phase characteristic prediction of reflect array antennas unit elements [11-14], for synthesis and analysis of microstrip lines [15,16], for modelling a microstrip patch designs [17-19], dielectric properties prediction of the vegetation [20], investigation the effects of aperture dimension ratio on electrical shielding effectiveness [21] and prediction of the radiated emission from heatsink's and heatsink optimization [22].

Herein, three different rail geometries have been simulated with three different armature types using ANSYS Maxwell which is based on 3-D Finite Element Method to determine effective railgun geometries. After one of the best geometries was determined, geometrical parameters such as rail length, separation between the rails, rail radius, armature height and armature length were changed on this railgun's model and this railgun's performance was observed and measured on the simulation environment. Then based on the obtained simulated data, an Artificial Intelligence (AI) based surrogate model for railgun design to prevent time consuming and to make design optimization process computationally efficient is taken into the consideration. AI based surrogate model predicted railgun's output force with SMAPE of 1.89% and in milliseconds. Moreover, in the surrogate model, there is no need for drawing to see the output, it is sufficient to give only the model inputs. In ANSYS Maxwell software calculation time almost takes five minutes excluding railgun drawing (used computer properties: 16 Gb RAM, Intel Core i7 processor). Considering that hundreds of parameters are changed while making a design, it is seen that the surrogate model saves a lot of time. As an example design optimization study case, one of the commonly used meta-heuristic optimization algorithms Particle Swarm Optimization (PSO) had been used for data driven surrogate model assisted optimization process. Thus,

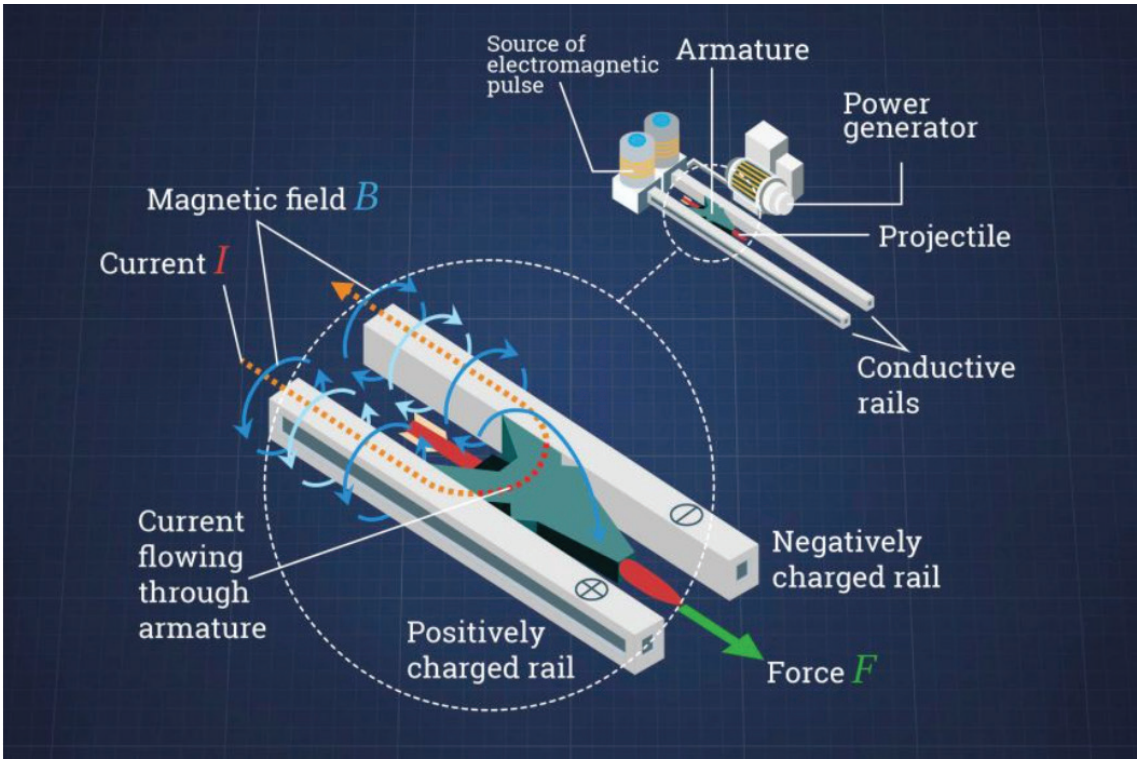

Figure 1. Railgun diagram [3].

by using AI based computational efficient surrogate modelling and Meta-Heuristic optimization algorithms; a fast, reliable, accurate and computational efficient optimization process has been achieved. In the next section, analysis of the proposed railgun design has been presented. In section 3, AI based surrogate modelling techniques for modelling of the proposed railgun design has been studied. In section 4, a study case for design optimization of railgun using AI based surrogate model has been presented, and finally the work ends with a brief conclusion in section 5.

ANALYSIS OF DIFFERENT RAILGUN GEOMETRIES

Related Equations

Maxwell's equations with the Ampere law in differential form when the displacement current is neglected [23];

$$\nabla \times \vec{H} = \vec{J} + \vec{J}_e \tag{1}$$

Where H is magnetic field intensity and J is impressed current density. In some case the equality $\vec{J}$ must be replace by $\vec{J} + \vec{J}_e$ where $\vec{J}_e$ is eddy current. Non-existence of magnetic charges in differential form that is shown in following equation [24];

$$\nabla \cdot \vec{B} = 0 \tag{2}$$

Using equation 2, can be written B is curl A;

$$\nabla \times \vec{A} = \vec{B} \Rightarrow \vec{H} = \frac{1}{\mu} \nabla \times \vec{A} \tag{3}$$

Where $\vec{B}$ and μ are magnetic flux density and permeability respectively, the induced eddycurrent is given by [25];

$$\vec{J}_e = \sigma \vec{E} \tag{4}$$

$$\vec{J}_e = -\sigma \frac{\partial \vec{A}}{\partial t} \tag{5}$$

Where σ and $\vec{E}$ are conductivity and electrical field respectively. The differential equation for the magnetic vector potential $\vec{A}$ in transient case is;

$$\nabla \times \left(\frac{1}{\mu} \nabla \times \vec{A} \right) + \sigma \frac{\partial \vec{A}}{\partial t} = \vec{J} \tag{6}$$

The interaction between the magnetic field density produced by the rail's current in the place of the armature and the passing current of the armature causes its acceleration along the rails. This force is obtained from the Lorentz law [26];

$$\vec{F} = \vec{J} \times \vec{B} \quad \text{(N)} \tag{7}$$

Inductance gradient is defined as the ratio of magnetic energy per length to current square. Then we can write [27];

$$L = 2(F/I^2) \text{ (H/m)} \tag{8}$$

where L, I and F are the inductance gradient, injected current and the applied force to the armature respectively.

Inductance gradient is a function of railgun dimensions and the rail material, also a useful parameter that used to show the efficiency of the railgun. Therefore, there are many studies on the effects of rail and armature geometry [28], [29], [30] and materials [25] on the inductance gradient.

SIMULATION MODEL PARAMETERS

Geometry And Material

Square, triangular and half-cylindrical rails were selected as different rail geometries. C type, rectangular and hollow types of armature geometries were selected as different armature geometries. Inner side of the rails are preferred flat shape because of its advantages such as high inductance gradient, easy cleaning, easy maintenance, easy removing and loading, lower cost and uniform field distribution [29]. The rail pairs have been shown in Figure 2 below.

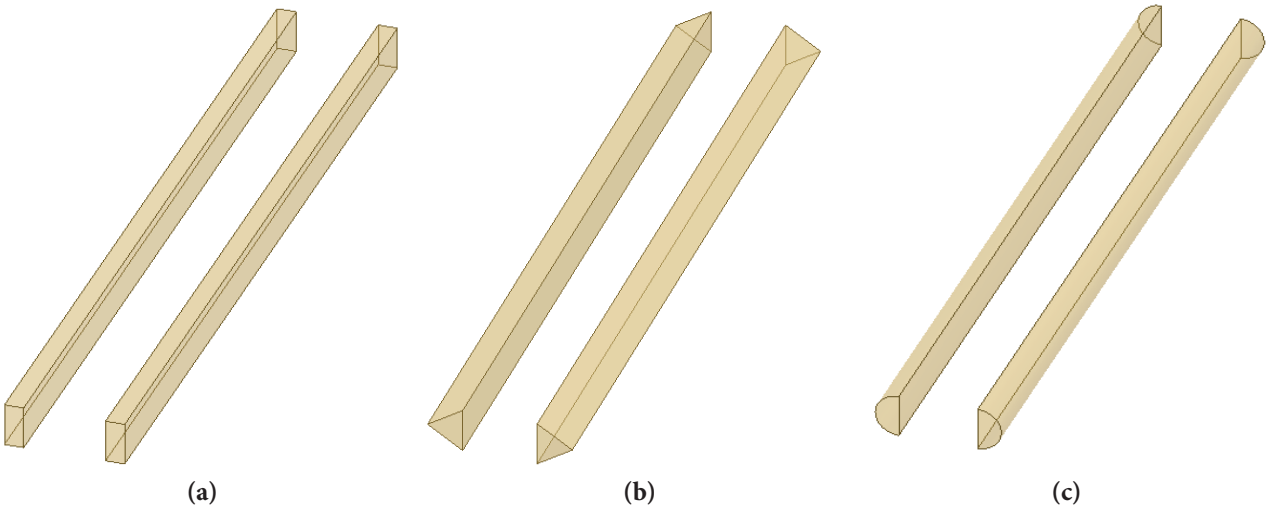

(a) (b) (c)

Figure 2. Rail geometries: (a) rectangular, (b) triangular, (c) half-cylindrical rail

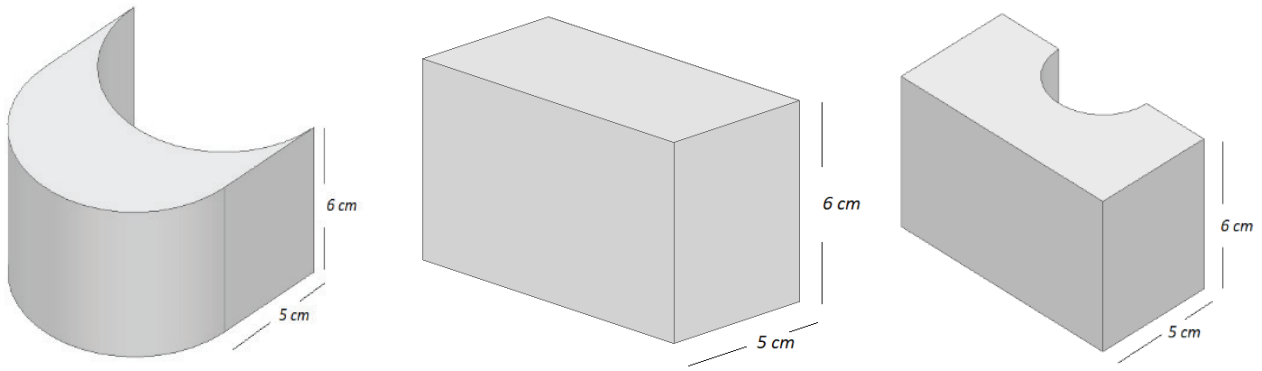

Figure 3. Armature geometries: (a) C-type, (b) rectangular, (c) hollow type armatures.

There are different options of possible armature designs, but the most common and most studied designs are the so-called C-type armatures and brush armatures [31,32]. For this reason C-type armature was chosen firstly for analysis. Secondly, a rectangular armature with the same volume as the C-type was designed to examine the volume effect. Lastly, a hollow-type armature which is between C-type and rectangular geometry as a similarity was designed to examine the surface area effect. The armature geometries have been shown in Figure 3 below.

There is a direct relationship between the performance, service life, reliability, the cost and the material of railgun. According to high Roche quality factor of materials; rail material is widely selected the copper alloy or composites, armature material is selected aluminum with the lower density [33]. Therefore, in this study material has been chosen copper for rail and aluminum for the armature.

In order to analyze effects of railgun geometry on the output force, all simulation parameters have been taken equal except geometrical variations.

Each rail has 100 cm length, 6 cm height and equal rail cross section (14.13 cm^2) which is adjusted according to the half cylindrical rail radius (r = 3 cm). Each rail type has the same volume of 1413 cm^3. According to these design parameters; the surface areas of the cylindrical, rectangular and triangular rails were 1570 cm^2, 1700 cm^2 and 1745 cm^2 respectively.

Railgun calibrations were designed equally; rail separations were fixed to 10 cm and each armature's width was fixed to 10 cm for creating a conduction path between rails. Armature height was taken 6 cm that is equal to the rail height.

C type armature and rectangular armature types were designed with equal volumes (300 cm^3), as hollow and rectangular types have equal surface area (280 cm^2) to observe whether surface area and volume has an effect on the output force. The detailed armature design properties were given below in Table 1.

Input Current and Distributions

Divinilbenzene Skin effect causes gaps on the material, these gaps may result in high-voltage discharge and ablation on the surface of rails and armature [34]. Uniformity of the current distribution reduces the harmful effect of the skin effect effectively. Material and thickness of the railgun effect the current distribution and uniformity on the rails. Creating railgun material using thin layers increases the uniformity, reduces the harmful effects [35]. Based on advances in uniformity studies and since we want to examine only the effect of geometry variations on the output force, input current was adjusted 100 kA as a constant value along the rails. Because of the constant input current, output force and inductance gradient have the same effect on evaluating the railgun's performance. (Eq. 9). Current density graph of Half-cylindrical rail - C type armature pair has been given in Figure 4 in below for an example.

Table 1. Armature Properties [cm]

Armature Type	Rail Intersection	Height	Surface Area	Volume
C type	5	6	348.5	300
Rectangular	5	6	280	300
Hollow	5	6	280	255

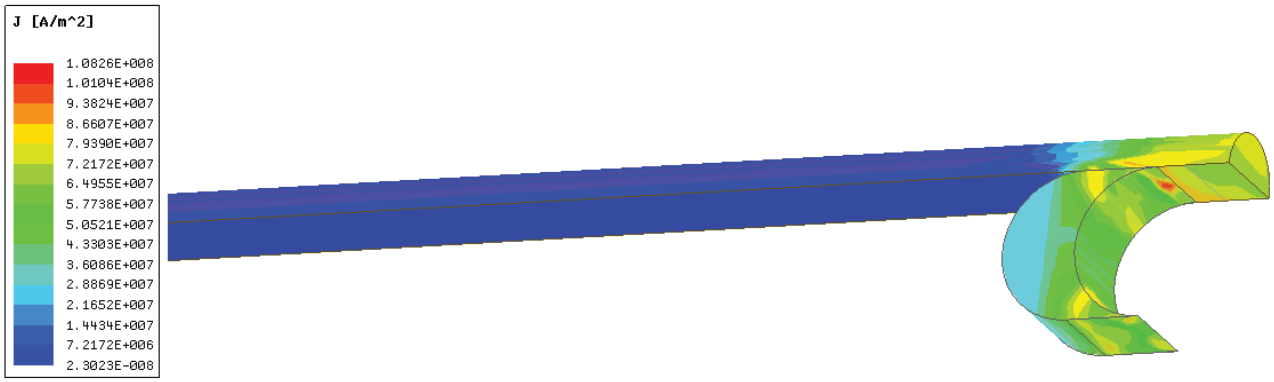

Figure 4. Current density graph of Half-cylindrical rail - C type armature pair.

Simulation Results

Ansys Maxwell software provides 2D and 3D low frequency electric field simulation for analysis of electromagnetic and electromechanical devices.

Three rail geometries have been simulated three different armature types, totally nine different cases were observed. Armatures were moved parametrically along the rails and calculations have been carried out by using ANSYS software that based on 3-D Finite Element Method (FEM). FEM is a numerical technique that divides the modeled geometry to the finite elements and solves the problem partially. In analysis, surface approximation based mesh structure was selected for Half-cylindrical rail and length based mesh structure was selected for other armature and rail geometries. Same amount of mesh cells was used for the same geometry in different simulations.

The inductance gradient has been calculated for each scenario, armature dependent graphics for each rail has been shown in Figure 5.

It is seen from Figure 5 that inductance gradient values directly dependent the rail-armature geometry. The output force of the triangular rail geometry is stable and does not fluctuate along the rail. The average of inductance gradient values along the rails are shown in Table 2.

Due to the skin effect, current tends to flow on the outer surfaces of the conductors during the early launch period. And in the following launch period, current is concentrated on the outer surface by the velocity skin effect (VSE) [31]. Since all rails' inner surfaces where the current flows [34] to the armature are the same, the armature with a large surface area is expected to provide better inductance gradient.

As seen in Table 2, C type armature has the highest inductance gradient for all cases. When the inductance gradient is evaluated in terms of surface area; C-type armature with high surface area has given better inductance gradient in all situations. Rectangular and hollow type armatures with same surface area as each other but with a lower surface area than C type armature have given the same inductance gradient with each other but lower than C type armature.

Between the C-type and rectangular type armatures with the same volume but different surface areas; C type with a high surface area has given higher inductance gradient. Besides, between the rectangular and hollow type armatures with the same surface area but different volumes; they have given almost same inductance gradient.

Also, it is seen that from Table 2, the same armature type gives different inductance gradient values in combination with different rail types, so we can say that not only the armature geometry, but also the rail geometry has effect on the inductance gradient.

AI Based Surrogate Modelling Techniques for the Output Force Prediction

Half-cylindrical rail - C type armature pair was selected for AI based surrogate modelling. This pair's geometric variables are shown in Figure 6. This model was analyzed with the geometric values that are given in the Table 3. According to the variables in the Table 3, 486 combinations were created. Therefore, 486 independent simulations were carried out. Simulation results were saved to create train and test dataset for the surrogate models.

Artificial Intelligence based surrogate model is a concept that allows the machine to learn from data and experiences with using algorithms. These models gain the ability to prediction and classify by examining and learning the previous cases [36]. That's why surrogate models can predict or classify new cases with very high accuracy and easily.

The output force predictions of railguns whose dimensions are not within the trained models' dimension range will not be correct. For example, accurate predictions will not be obtained for rail lengths of more than 200 cm, less than 100 cm or armature height of more than 11 cm, less than 1 cm. Therefore, the output force predictions of the model will be within the limits of the trained data. If the user wants predictions in a wider or tight range, the train data should be created in this scope of range as well.

Since each algorithm doesn't suitable for every problem and we do not know whether the dataset has linear or non-linear attribute, we trained our data with six different

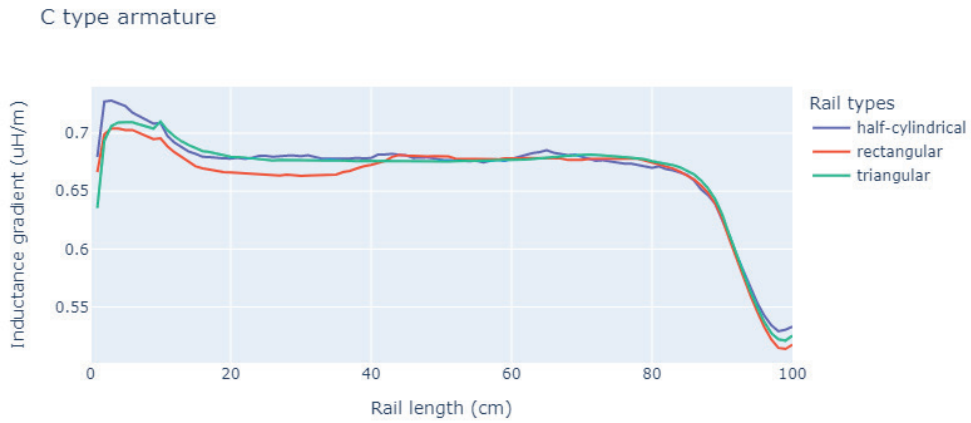

(a)

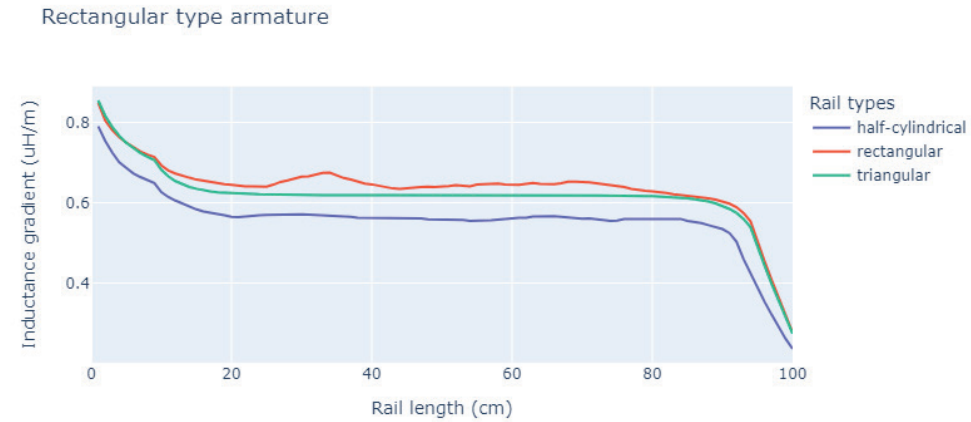

(b)

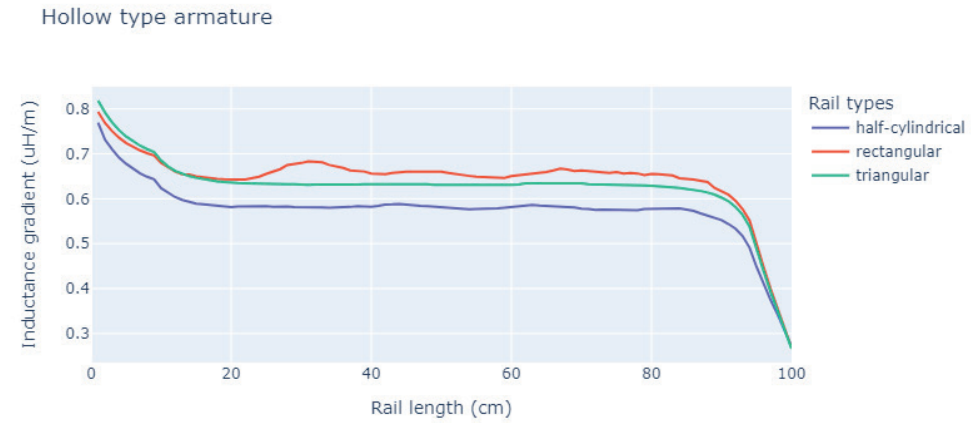

(c)

Figure 5. Inductance gradient graphs.

Table 2. Average inductance gradient values (uH/m).

Armature Types	Half-cylindrical rail	Rectangular rail	Triangular rail
C type	0.68	0.67	0.68
Rectangular	0.57	0.65	0.62
Hollow	0.58	0.65	0.63

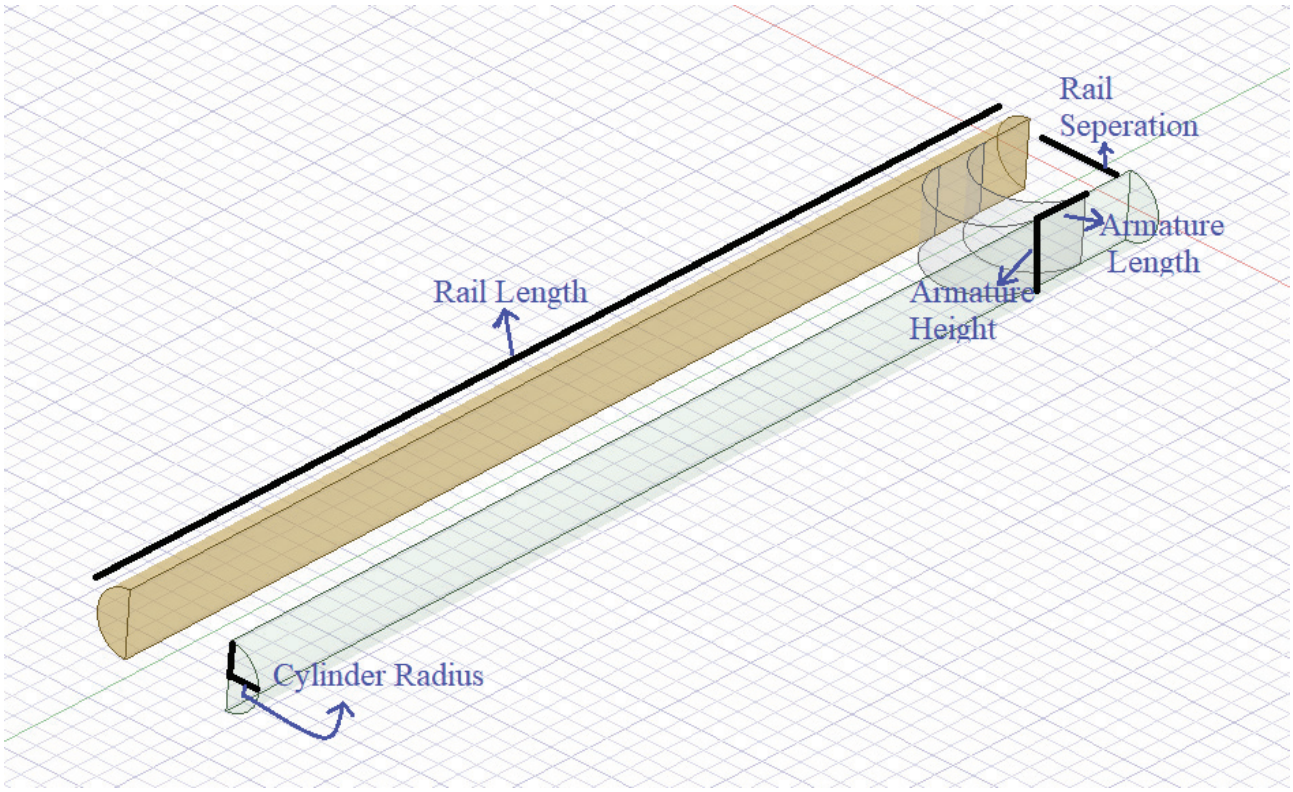

Figure 6. Railgun geometric variables.

Table 3. Geometric variables and dataset inputs

Input Parameters	Values [cm]
Rail Length (Rail_L)	100 - 150 - 200
Rail Separation (Seperation)	5 -10 -15
Cylinder Radius (Cyl_Rad)	1 - 3 - 5
Armature Length (Arm_L)	1 - 3- 5
Armature Height (Arm_H)	1 - 3- 5 - 7 - 9 - 11
Total number of combinations	486

techniques to determine the best surrogate model for our dataset.

Used techniques are;

- Artificial Neural Network (ANN)
- Support Vector Regression (SVR)
- Random Forests
- XGBoost
- K Nearest Neighborhood (KNN)
- Multiple Linear Regression (MLR)

Dataset was divided by 0.25 test data and 0.75 train data. Some examples of the dataset are given in Table 4. After model tuning, surrogate models were trained and tested using Keras and Scikit-Learn frameworks on Python 3.7 environment.

Model tuning parameters and best parameters are given in Table 5. When model tuning stage, it is difficult to manually change the hyper parameters. Therefore, GridSearchCV method was used. GridSearchCV is a sklearn's library function. With this method, training was carried out by cross-matching with all hyperparameters that is wanted to be combine each other. Then the parameters which we get the best result were added to the best parameter column in the Table 5.

Table 4. Some examples of dataset

Armature Height [cm]	Armature Length[cm]	Cylinder Radius[cm]	Rail Length [cm]	Rail Separation [cm]	Output Force (kNewton)
7	1	5	100	5	2.23
11	5	3	150	15	4.08
9	3	5	200	10	2.84

In all methods, input data was normalized using the minimum and maximum value of input data (as in equation 9). The normalized data was given as input to model for prediction.

$$y' = \frac{y - min_y}{max_y - min_y} \quad (9)$$

In order to evaluate model accuracy, there are many measurement techniques [37]. In this study root mean square error (RMSE) (as in equation 10) and symmetric mean absolute percentage error (SMAPE) (as in equation 11) [37] were used for evaluation.

$$RMSE = \sqrt{\frac{1}{n}\sum_{j=1}^{n} \left(y_j - \hat{y}_j\right)^2} \quad (10)$$

$$SMAPE = \frac{1}{n}\sum_{j=1}^{n} \frac{100 * |y_j - \hat{y}_j|}{(|y_j| + |\hat{y}_j|)/2} \quad (11)$$

Table 5. Model tuning parameters

Model	Used parameters for model tuning with GridSearchCV method	Best Parameters
ANN	cross validation=5, estimator=MLPRegressor, activation functions ='identity', 'logistic', 'tanh', 'relu','elu', 'selu', 'exponantial', epochs=500 with early_stopping= True, hidden_layer_sizes: 10, 15, 20, 30, (10, 15), (15, 20), (20, 20), (20, 30), (60, 90), (100, 20), (10, 15, 20), (15, 20, 30), (20, 20, 20), (50, 50, 50), (30, 90, 120), (120, 90, 30), (100, 50, 150), (300, 200, 150), dropout: 0.2, 0.3, 0.5, False, optimizer: 'SGD', 'RMSprop', 'Adagrad', 'Adadelta', 'Adam', 'Ftrl', 'Adamax', 'Nadam' Other parameters are used as default depend on the above parameters	Activation func = 'relu', hidden_layer_size = (300, 200, 150), dropout = False, optimizer = 'Adam'
SVR	cross validation=5, estimator= SVR (cache_size=200, coef0=0.0, degree=3, epsilon=0.1, gamma='scale', kernel='rbf', max_iter=-1, shrinking=True, tol=0.001), 'C': [0.1, 0.4, 3, 5, 20, 10000, 20000, 100000]	Regularization parameter (C) = 10000
Random Forests	cross validation=5, estimator = RandomForestRegressor (bootstrap=True, ccp_alpha=0.0, criterion='mse', max_depth=None, max_features='auto', max_leaf_nodes=None, max_samples=None, min_impurity_decrease=0.0, min_impurity_split=None, min_samples_leaf=1, min_samples_split=2, min_weight_fraction_leaf=0.0), 'max_depth': [1, 2, 3, 4, 5, 6, 7, 8, 9], 'max_features': [2, 3, 4], 'n_estimators': [50, 100, 200, 500, 1000, 2000]}	max_depth = 8, max_features =4, n_estimators = 2000
KNN	cross validation=5, estimator = KNeighborsRegressor (algorithm='auto', leaf_size=30, metric='minkowski', metric_params=None, n_neighbors=5, p=2, weights='uniform'), 'n_neighbors': [1, 2, 3, 4, 5, 6, 7, 8, 9, 10, 11, 12, 13, 14, 15, 16, 17, 18, 19, 20, 21, 22, 23, 24, 25, 26, 27, 28, 29]	n_neighbors = 2
XGBoost	cross validation=5, estimator = XGBRegressor (base_score=None, booster=None, colsample_bylevel=None, colsample_bynode=None, colsample_bytree=None, gamma=None, importance_type='gain', interaction_constraints=None, learning_rate=None, max_delta_step=None, max_depth=None, min_child_weight=None, missing=nan, monotone_constraints=None, reg_lambda=None, scale_pos_weight=None, subsample=None, tree_method=None, validate_parameters=None, 'colsample_bytree': [0.4, 0.5, 0.7, 0.9, 1], 'learning_rate': [0.001, 0.01, 0.1, 0.2, 0.5], 'max_depth': [2, 3, 4, 5, 8], 'n_estimators': [100, 200, 500, 1000]	colsample_bytree = 0.7 learning_rate = 0.1, max_depth = 3, n_estimators = 1000
MLR	Method : Least Squares LinearRegression (fit_intercept=True) There are no parameters to tune	Method : Least Squares LinearRegression (fit_intercept=True)

Table 6. Prediction results

Model	SMAPE (%)	RMSE
Artificial Neural Network (ANN)	average: 1.89	average: 0.126
	std.dev:0.05	std.dev:0.001
Multiple Linear Regression	11.44	2.03
Support Vector Regression (SVR)	3.57	0.2
Random Forests	average: 2.37	average: 0.175
	std.dev:0.06	std.dev:0.003
K Nearest Neighborhood (KNN)	7.21	0.412
XGBoost	1.96	0.1347

Where y' normalized input, y_j, $\hat{y}_j$ are actual and predicted values and n is the number of input respectively.

Prediction results are shown in Table 6. Since ANN and Random Forests models' outputs change with every model fitting, 10 independent fitting were carried out for these models and their averages were given with their standard deviations.

Besides, to compare predictions of the best and the worst surrogate model, prediction graphs were given in Figure 7. Test data (0.25 of entire dataset) was used for target data in mentioned predictions.

OPTIMIZATION

PSO is one of the widely used traditional optimization algorithms, has been used in the Matlab environment for a selected cost function. For the last decades, Meta-Heuristic Algorithms (MHA) has been extensively used as an efficient solution method for finding optimal results in design optimization process of many microwave devices [38-48]. Due to their unique heuristic search methods, these algorithms can be efficiently used in for solving non-differentiable or discontinuous, non-convex, and highly nonlinear problems that might not be solved with gradient based algorithms [5].

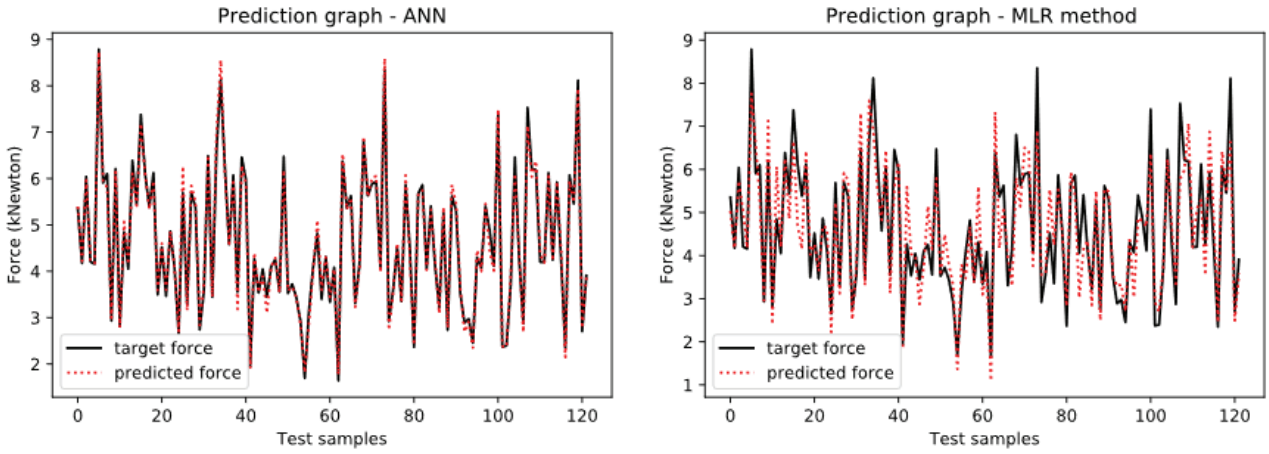

Figure 7. Prediction graphs.

Table 7. Optimization results

Input Optimization with Partical Swarm Optimization(PSO) for 8.0 kNewton Output Force								
Iteration	*Population*	*Inputs [cm]* Arm_H	Arm_L	Cyl_Rad	Rail_L	Seperation	Optimization Result (kN)	Ansys Result (kN)
10	*30*	1	5	1	142	12.7	7.99	7.93
10	*50*	1	1	1	100	7	7.99	8.06
10	*100*	1	5	1	100	14.4	7.99	7.98
30	*30*	1	5	1	200	10.5	8	8.07
30	*50*	1	5	1	100	14.4	8	7.98
30	*100*	1	5	1	200	10.5	8	8.07
50	*30*	1	5	1	200	10.5	8	8.07
50	*50*	1	5	1	100	14.4	8	7.98
50	*100*	1	5	1	200	10.5	8	8.07

The PSO algorithm tries to reach the optimum point by minimizing the cost function. Input parameters that create the predicted force are continuous in the optimization process, it doesn't have to be discrete as it is seen in Table 7. Used cost function is given in equation 12 below.

$$C = |required\ force - predicted\ force| \quad (12)$$

In the dataset that we use for this model, railgun's output force range is between 1.62 kNewton and 9.54 kNewton. For this reason, while performing PSO optimization, this range was not exceeded. This optimization is able to work in this range, but we just optimized only 8.0 kNewton for the sample in the study.

Required inputs for 8.0 kNewton required output force were found using PSO algorithm with 30, 50, 100 populations. Moreover, number of iterations were examined to see the convergency of the algorithm. Optimization results have been compared with Ansys outputs in Table 7. As seen in Table 7; at first, PSO reached 7.99 kNewton with 30 population and 10 iterations, after this point increasing the population size did not change the result but increasing the iterations to 30 converged the result to 8.0 kNewton.

CONCLUSION

We simulated and analyzed the three rails geometry and the three types of armature to obtain high inductance gradient for achieving higher output force and so higher projectile velocities.

Simulation results show that C type armature provides best inductance gradient with all type of rails. Although the volume of the armature is not effective on the output force, it was seen that the surface area of the armature is effective. While C type armature with high surface area has given better performance in all situations, rectangular and hollow type armatures with low surface area has given lower and almost same performance as each other.

Results validate that there is a dependency between the effectiveness of railgun and its geometry. After creating a dataset, railgun electromagnetic force can be predicted with the surrogate model algorithms easily, without the need to repeatedly draw and simulate.

Surrogate model prediction results show that Artificial Neural Network, XGBoosts and Random Forests methods are very successful for our dataset. They achieved railgun electromagnetic output force prediction with minimum SMAPE of 1.89%, 1.96% and 2.37% respectively.

Also, PSO showed that we can easily determine the railgun geometry inputs to get the desired output force. In this way; quick, easy and low-cost analyses can be done before production.

Further analysis on the effects of hyper parameters was not studied in this work since the proposed method already achieved acceptable results. However, in future works for design problems with higher non-linearity characteristics between inputs and outputs alongside a wider range of variables, optimization and optimal determination of hyper-parameters for surrogate model is a must and will be taken into the consideration in future works of the authors.

AUTHORSHIP CONTRIBUTIONS

Authors equally contributed to this work.

DATA AVAILABILITY STATEMENT

The authors confirm that the data that supports the findings of this study are available within the article. Raw data that support the finding of this study are available from the corresponding author, upon reasonable request.

CONFLICT OF INTEREST

The author declared no potential conflicts of interest with respect to the research, authorship, and/or publication of this article.

ETHICS

There are no ethical issues with the publication of this manuscript.

REFERENCES

[1] Çevik Y. Modeling of an electromagnetic launcher (master thesis). Ankara: Middle East Technical University; 2015.

[2] Murugan R, Udayakumar K. Effect of rail dimensions on rail gun design parameters. 2005 Annual IEEE India Conference - Indicon, 2005; 623–626.

[3] Weedon A. What exactly is a railgun. Available at: https://www.abc.net.au/news/2019-01-03/the-railgun-explained-and-what-it-means-for-us-china-relations/10683526. Accessed on Dec 20, 2020.

[4] Mahouti P. Application of artificial intelligence algorithms on modeling of reflection phase characteristics of a nonuniform reflectarray element. Int J Numer Model Electron Networks Devices Fields 2019;e2689. [CrossRef]

[5] Mahouti P. Design optimization of a pattern reconfigurable microstrip antenna using differential evolution and 3D EM simulation-based neural network model. Int J RF Microwave Comput Aided Eng 2019;29:e21796. [CrossRef]

[6] Giannini F, Leuzzi G, Orengo G, Albertini M. Small-signal and large-signal modeling of active devices using CAD-optimized neural networks. Int J RF Microwave Comput Aided Eng 2002;12:71–78. [CrossRef]

[7] Marinković Z, Markovic V. Temperature-dependent models of low-noise microwave transistors based on neural networks. Int J RF Microwave Comput Aided Eng 2005;15:567–577. [CrossRef]

[8] Güneş F, Mahouti P, Demirel S, Belen MA, Uluslu A. Cost-effective GRNN-based modeling of microwave transistors with a reduced number of measurements. Int J Numer Model Electron Networks Devices Fields 2017;30:e2089. [CrossRef]

[9] Belen MA, Güneş F, Mahouti P, Demirel S. Signal and noise modeling of microwave transistors using characteristic support vector-based sparse regression. Radioengineering 2016;25:490–499. [CrossRef]

[10] Marinković Z, Crupi G, Caddemi A, Markovic V, Schreurs D. A review on the artificial neural network applications for small-signal modeling of microwave FETs. Int J Numer Model Electron Networks Devices Fields 2020;33:e2668. [CrossRef]

[11] Güneş F, Demirel S, Mahouti P. Design of a front-end amplifier for the maximum power delivery and required noise by HBMO with support vector microstrip model. Radioengineering 2014;23:134–143.

[12] Güne F, Dem S, Rel, Nes S. A novel design approach to x-band minkowski reflectarray antennas using the full-wave EM simulation-based complete neural model with a hybrid ga-nm algorithm. Radioengineering 2014;23:144–153.

[13] Mahouti P, Güneş F, Belen MA, Çalışkan A. A novel design of non-uniform reflectarrays with symbolic regression and its realization using 3-D printer. Aces Journal 2019;34:280–285.

[14] Mahouti M, Kuskonmaz N, Mahouti P, Belen MA, Palandoken M. Artificial neural network application for novel 3D printed nonuniform ceramic reflectarray antenna. Int J Numer Model Electron Networks Devices Fields 2020;33:e2746. [CrossRef]

[15] Krishna D, Narayana J, Reddy D. ANN models for microstrip line synthesis and analysis. world academy of science, engineering and technology, international science index 22. Int J Electr Comput Energetic Electron Commun Eng 2008;2:2343–2347.

[16] Mahouti P, Gunes F, Belen MA, Demirel S. Symbolic regression for derivation of an accurate analytical formulation using big data: an application example. Aces Journal 2017;32:574–591.

[17] Karaboga D, Guney K, Sağiroğlu Ş, Erler M. Neural computation of resonant frequency of electrically thin and thick rectangular microstrip antennas. IEE Proc Microwave Antennas Propag 1999;146:155–159. [CrossRef]

[18] Mishra RK, Patnaik A. Neural network-based CAD model for the design of square-patch antennas. IEEE Trans Antennas Propag 1998;46:1890–1891. [CrossRef]

[19] Çalik N, Belen MA, Mahouti P. Deep learning base modified MLP model for precise scattering parameter prediction of capacitive feed antenna. Int J Numer Model Electron Networks Devices Fields 2020;33:e2682. [CrossRef]

[20] Metlek S, Kayaalp K, Basyigit I, Genc A, Dogan H. The dielectric properties prediction of the vegetation depending on the moisture content using the deep neural network model. Int J RF Microwave Comput Aided Eng 2021;31:e22496. [CrossRef]

[21] Basyigit I, Dogan H. The analytical and artificial intelligence methods to investigate the effects of aperture dimension ratio on electrical shielding effectiveness. Int J Electron Telecommun 2019;65:359–365.

[22] Basyigit I, Genc A, Dogan H, Şenel FA, Helhel S. Deep learning for both broadband prediction of the radiated emission from heatsinks and heatsink optimization. Eng Sci Technol Int J 2021;24:706–714. [CrossRef]

[23] Plonus MA. Applied electromagnetic. McGraw-Hill Publishing Company, New York; 1978.

[24] Bayati M, Keshtkar A, Makki SV. Analyzing the current distribution, magnetic field and inductance gradient at the circular rail in comparison to rectangular rail. 2012 16th International Symposium on Electromagnetic Launch Technology; 2012; 1–5. [CrossRef]

[25] Bayati S, Keshtkar A. Effect of Rail's material on railgun inductance gradient and losses. 2008 14th Symposium on Electromagnetic Launch Technology; 2008; 1–4. [CrossRef]

[26] Keshtkar A, Mozaffari S. Inductance gradient variation with time and armature sliding along the rails. IEEE Trans Plasma Sci 2011;39:75–79. [CrossRef]

[27] Keshtkar A. Effect of rail dimension on current distribution and inductance gradient. 2004 12th Symposium on Electromagnetic Launch Technology; 2004; 359–362.

[28] Kerrisk J. Current distribution and inductance calculations for rail-gun conductors. Technical Report. Report No: LA-9092-MSON: DE82007033. Los Alamos National Lab., NM (USA).

[29] Marshall RA. Railgun bore geometry, round or square. Proc IEEE Trans Magn 1999;35:427–431. [CrossRef]

[30] Yadong Z, Jiang-jun R, Yuanchao H, Ruohan G, Wu W. Ablation and geometry change study of solid armature in a railgun. Chin Phys B 2013;22:084102. [CrossRef]

[31] Kim B, Hsieh K. Effect of rail/armature geometry on current density distribution and inductance gradient. IEEE Trans Magn 1999;35:413–416. [CrossRef]

[32] Chen L, He J, Xia S, Yuan Z, He H. Some key parameters of monolithic C-type armature in rectangular caliber railgun. IEEE Trans Plasma Sci 2017;45:1465–1469. [CrossRef]

[33] Du C. Analysis of materials selection for electromagnetic railguns. 5th International Conference on Machinery, Materials and Computing Technology, Advances in Engineering 2017; 126. [CrossRef]

[34] Zuo P, Li J, Song X, Yuan J. Characteristics of current distribution in rails and armature with different section shape rails. IEEE Trans Plasma Sci 2013;41:1488–1492. [CrossRef]

[35] Xing Y, Lv Q, Lei B, Xiang H, Zhu R, Liu C. Analysis of transient current distribution in copper strips of different structures for electromagnetic railgun. IEEE Trans Plasma Sci 2015;43:1566–1571. [CrossRef]

[36] Shalev-Shwartz S, Ben-David S. Understanding Machine Learning - From Theory to Algorithms. Cambridge: Cambridge University Press; 2014. [CrossRef]

[37] Hyndman R, Koehler A. Another look at measures of forecast accuracy. Int J Forecasting 2006;22:679–688. [CrossRef]

[38] Güneş F, Demirel S, Mahouti P. A simple and efficient honey bee mating optimization approach to performance characterization of a microwave transistor for the maximum power delivery and required noise. Int J Numer Model Electron Networks Devices Fields 2016;29:4–20. [CrossRef]

[39] Zheng S. The applications of jumping genes inspired evolutionary algorithms in microwave circuit designs. 2017 International Applied Computational Electromagnetics Society Symposium (ACES); 2017; 1–2.

[40] Guney K, Onay M. Bees algorithm for design of dual-beam linear antenna arrays with digital attenuators and digital phase shifters. Int J RF Microwave Comput Aided Eng 2008;18:337–347. [CrossRef]

[41] Galehdar A, Thiel D, Lewis A, Randall M. Multiobjective optimization for small meander wire dipole antennas in a fixed area using ant colony system. Int J RF Microwave Comput Aided Eng 2009;19:592–597. [CrossRef]

[42] Zheng S, Yeung S, Chan W, Man K, Tang W. Design of broadband hybrid coupler with tight coupling using jumping gene evolutionary algorithm. IEEE Trans Ind Electron 2009;56:2987–2991. [CrossRef]

[43] Güneş F, Belen MA, Mahouti P. Competitive evolutionary algorithms for building performance database of a microwave transistor. Int J Circuit Theory Appl 2018;46:244–258. [CrossRef]

[44] Yıldırım A, Güneş F, Belen MA. Differential evolution optimization applied to the performance analysis of a microwave transistor. Sigma J Eng & Nat Sci 2017;8:135–144.

[45] Clark H, Jeong N, Jeong S. Concurrent gain and bandwidth improvement of a patch antenna with a hybrid particle swarm optimization algorithm. 2019 IEEE 20th Wireless and Microwave Technology Conference (WAMICON); 2019; 1–3. [CrossRef]

[46] Rahmat-Samii Y. Modern antenna designs using nature inspired optimization techniques: let Darwin and the bees help designing your multi band MIMO antennas. 2007 IEEE Radio and Wireless Symposium; 2007; 463–466. [CrossRef]

[47] Patel P, Kumari G, Saxena P. Array pattern correction in presence of antenna failures using metaheuristic optimization algorithms. 2019 International Conference on Communication and Signal Processing (ICCSP); 2019; 0695–0700. [CrossRef]

[48] Grewal NS, Rattan M, Patterh M. A linear antenna array failure detection using Bat Algorithm. 2015 Eighth International Conference on Contemporary Computing (IC3); 2015;202–207. [CrossRef]